Dynamic Response of Non-Ballasted Slab Tracks With CAM and SFRC Under High-Speed Rail Loading

Nilay Anand[1], Alok Kumar Ray[2*]

[1] Researcher, Tata Steel Limited, Jamshedpur, Jharkhand, India-831014

[2] Assistant Professor, National Institute of Technology Jamshedpur, Jharkhand, India-831014

[*]Corresponding Author

DOI: https://dx.doi.org/10.51584/IJRIAS.2026.11030058

Received: 11 March 2026; Accepted: 16 March 2026; Published: 09 April 2026

ABSTRACT

This study presents a comprehensive numerical investigation of the dynamic thermo-mechanical behavior of non-ballasted slab track systems incorporating Cement Asphalt Mortar (CAM) and Steel Fiber Reinforced Concrete (SFRC) under high-speed rail (HSR) loading conditions. A three-dimensional finite element framework is developed to simulate coupled effects of moving wheel loads, thermal gradients, and material nonlinearity. The fatigue life of the CAM layer and the structural performance of SFRC-based slab tracks are systematically evaluated.

Results indicate that the CAM layer experiences a maximum compressive stress of 0.31 MPa under dynamic loading, corresponding to an exceptionally high fatigue life of 167.21 million axle repetitions, significantly exceeding the design requirement. Incorporation of SFRC reduces the peak compressive stress in CAM to 0.22 MPa and limits long-term plastic deformation to 0.138 mm, compared to 0.187 mm in conventional reinforced slabs. The maximum vertical and lateral displacements are 0.114 mm and 0.283 mm, respectively, which are well within the permissible limits specified by HSR standards. Furthermore, SFRC exhibits improved damage resistance, with substantial reductions in tensile and compressive damage in the slab.

Keywords: High-speed rail, Slab track, Cement Asphalt Mortar (CAM), Steel Fiber Reinforced Concrete (SFRC), Fatigue life, Finite element analysis, Dynamic response.

INTRODUCTION

The rapid expansion of global high-speed rail (HSR) networks has intensified the demand for advanced track systems that combine durability, low maintenance, and optimal performance under dynamic loading conditions. As conventional ballasted tracks face limitations in meeting these requirements, non-ballasted slab track systems have emerged as a superior alternative, leveraging innovative materials such as Cement Asphalt Mortar (CAM) and Steel Fiber Reinforced Concrete (SFRC) to enhance structural resilience. Mu et al. demonstrated that steel fiber content substantially affects slab shear resistance, with 1D-SFRC, 2D-SFRC, and JD-SFRC round slabs exhibiting 14%, 15%, and 24% greater ultimate shear strength, respectively, compared to conventional RD-SFRC slabs containing 1% fiber volume [1]. Wang et al. systematically evaluated how fiber characteristics (type, content, geometry, length, alignment, and hybrid combinations) affect the tensile performance of Ultra-high Performance Concrete (UHPC)[2].

Hou et al. employed point-cloud matching to analyze fracture surface heterogeneity in SFRC, identifying the root-mean-square of directional derivatives (Z_{2-3D}) as a critical indicator of fracture morphology and material heterogeneity [3]. Xue et al. compared the mechanical properties between aligned and randomly distributed fibers through tensile, flexural, and compressive tests, confirming superior strength in oriented fiber UHPFRC [4].

Yang et al. performed parametric studies on 3D-printed SFRC, revealing distinct failure modes corresponding to different fiber alignment patterns under compression and tension[5]. Zhang et al. investigated how fly ash and silica fume modify SFRC performance, noting that these additives differentially reduce matrix porosity while enhancing workability [6]. Their subsequent work quantified improvements in slump, compressive strength, and tensile capacity when these supplementary materials were incorporated into UHSFRC[7].

Zhou et al. examined the influence of steel fibers on interfacial transition zones (ITZs), finding that high fiber concentrations (≥1.5%) notably diminish tensile strength, fracture energy, and toughness in these critical regions [8]. Jia et al. demonstrated that 1.5 vol% hooked-end fibers boost 3D-printed SFHSC's compressive strength by 8-40% depending on orientation [9].

Liu et al. showed that milled steel fibers increase concrete toughness by over 25% compared to conventional fibers [10]. At the same time, Yang et al. verified that optimized fiber alignment enhances shear capacity in GFRP-reinforced beams [11]. Zheng et al. comprehensively reviewed SFRC's mechanical behavior, constitutive modeling, and durability characteristics[12]. Rashidi et al. investigated the influence of steel fibers on the mechanical properties and behavior of concrete through a combination of numerical simulations and laboratory experiments. They developed a series of numerical models and validated them against experimental results, employing circular-shaped aggregates to ensure model accuracy [13]. Jayasooriya's comparison of tensile models showed that the End Tapered Four Linear Model had superior accuracy in predicting the flexural behavior of SFRC [14]. Altheoy documented significant property enhancements in UHPFRC containing nano-kaolin clay and double-hooked fibers [15]. Yu et al. visualized how uniform fiber distribution mitigates stress concentrations and retards cracking [16], while Yang et al. characterized the anisotropic behavior of aligned fiber UHPC through CT analysis [17]. Liu et al. established that casting orientation critically affects the strain-hardening properties of SIFCON containing arc-shaped and hooked-end fibers [18]. Alwesabi et al. incorporated recycled tire waste, such as tire rubber particles, into the concrete mix, thereby helping address the problem of accumulated tire waste. However, the inclusion of crumb rubber resulted in a significant reduction in mechanical properties [19].

Despite an extensive understanding of CAM and SFRC behavior in slab-track applications, critical research gaps remain. First, comprehensive fatigue-life assessments of CAM layers under combined thermal and dynamic loading conditions—particularly in high-speed rail environments—are limited in the current literature. Second, although SFRC has demonstrated superior mechanical properties in various structural applications, its performance as a replacement for conventional reinforcement in prestressed concrete slab tracks remains underexplored. Third, while random-fiber-distribution algorithms have been proposed, their practical implementation in large-scale structural components such as track slabs requires further validation.

This study addresses these gaps through (1) a rigorous numerical and analytical evaluation of CAM's fatigue life under realistic HSR loading conditions, demonstrating its long-term durability exceeds design requirements; (2) a systematic comparison between SFRC and traditional reinforced slabs, quantifying performance advantages in terms of stress reduction, deformation control, and damage mitigation (40% lower tensile damage); and (3) development of an advanced fiber distribution algorithm that ensures homogeneous 2% fiber volume fraction while eliminating weak zones in full-scale track slabs. By bridging these research gaps, this work provides critical insights for optimizing HSR track systems through innovative material applications and modeling approaches.

MATERIALS AND METHODOLOGY:

Material specifications

The study investigated two key materials for slab track systems:

- Cement Asphalt Mortar (CAM-I): Composition of Portland cement (0.9), asphalt emulsion (1.6), fine aggregates (2.0) with A/C ratio 0.6-1.2
- Steel Fiber Reinforced Concrete: Hooked-end steel fibers (L=40mm, Ø=0.9mm) at 2% volume fraction

Finite Element Modeling Framework

The accurate prediction of high-speed rail (HSR) track system performance requires sophisticated numerical modeling that captures the complex interactions among structural components, material behavior, and dynamic loading conditions. This section presents the comprehensive 3D finite element (FE) framework developed to analyze the mechanical response of non-ballasted slab tracks incorporating Cement Asphalt Mortar (CAM) and Steel Fiber Reinforced Concrete (SFRC). The proposed modeling approach addresses three critical challenges in HSR track analysis:

1. Multi-physics coupling: Simultaneous consideration of thermal gradients and dynamic wheel loads
2. Material nonlinearity: Proper representation of CAM's viscoelastic behavior and concrete damage mechanisms
3. Reinforcement complexity: Realistic modeling of randomly distributed steel fibers at scale

The developed framework integrates three key modeling components: (1) a detailed 3D representation of the track system geometry, (2) advanced material constitutive models calibrated to experimental data, and (3) validated loading/boundary conditions representing actual HSR operational scenarios. In this context, a high-speed railway (HSR) track system was modeled in ABAQUS, as shown in Fig. 1(a). The precast track slab was prestressed using the cooling method. The dimensions of a prestressed concrete slab are presented in Fig. 1(b). Spring-damper supports simulating fastener elasticity. The precast track slab is prestressed using the cooling method [20].

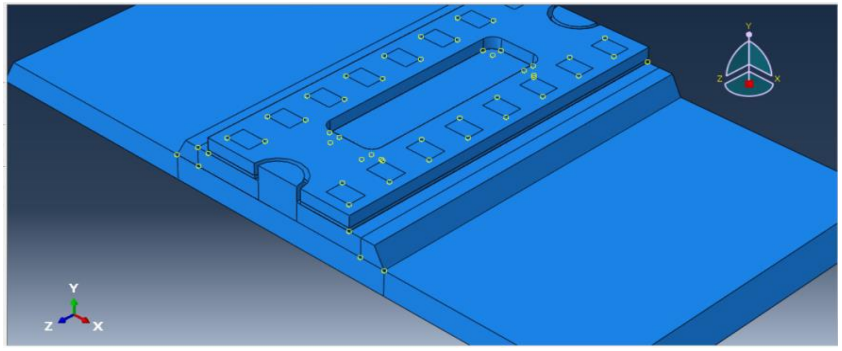

(a)

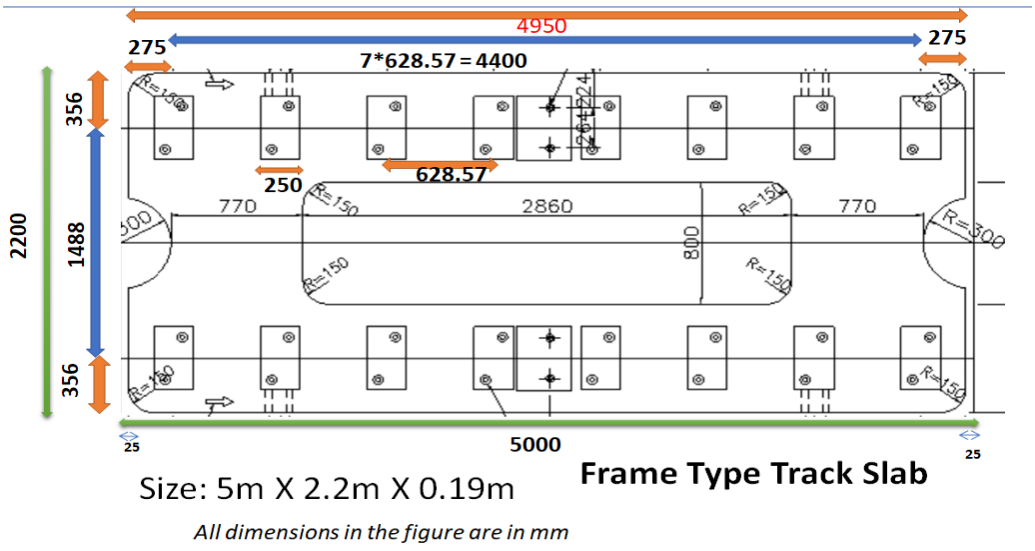

(b)

Figure 1: (a)3D FE model of railway track system and (b) Dimensions of prestressed concrete lab

Boundary and loading conditions

Boundary conditions

The finite element model incorporates realistic boundary conditions to accurately simulate the behavior of the high-speed rail (HSR) slab track system under operational loads. The following constraints are applied:

Rail-Slab Interaction

- The rail is modeled as a Timoshenko beam (UIC60 profile) and connected to the concrete slab via discrete elastic fasteners.
- Linear spring-damper elements simulate the fasteners with stiffness values derived from experimental data.

Slab-Subgrade Interface

- The bottom surface of the CAM layer is coupled to the subgrade using elastic foundation support (Winkler model).
- Subgrade stiffness is set to k = 0.05 GPa/m, consistent with typical HSR trackbed conditions.
- Viscous absorbing boundaries are applied at the lateral edges to minimize wave reflections.

Symmetry and Displacement Constraints

- Roller supports are applied at the longitudinal ends of the slab to allow thermal expansion while preventing rigid-body motion.
- Fixed constraints are imposed at the subgrade base to simulate bedrock support.

Loading Conditions

The model accounts for multiple loading scenarios to evaluate the track system's performance under realistic service conditions.

Thermal Loading

- Transient heat transfer analysis is performed to simulate daily temperature variations.
- Solar radiation flux (800 W/m²) is applied to the top surface, while convective cooling (h = 25 W/m²·K) represents ambient air effects.
- The thermal gradient is calibrated against meteorological data from Ahmedabad, India, yielding a peak $\Delta T = 12°C$ between the top and bottom slab surfaces.

Dynamic Wheel Loads

- Moving wheel load is applied as a Chinese hat pressure distribution with a peak magnitude of 175 kN (UIC standard for HSR).
- The load traverses the rail at 320 km/h, corresponding to a 30 Hz loading frequency.
- Track irregularities are modeled as a stationary Gaussian random process with power spectral density (PSD) per EN 13848-5.

Prestress Force Application

Prestress in the concrete slab is simulated via thermal contraction:

- A cooling temperature drop (ΔT = -35°C) is applied to prestressing tendons to induce 8.4 MPa effective compressive stress.
- A perfect bond between tendons and concrete is assumed.

Assumptions

The following assumptions are considered for the modelling:

1. CAM layer behaves as an Isotropic viscoelastic material

2. CAM properties are temperature-dependent but considered homogeneous within each layer

3. No aging effects are considered during the analysis period for the CAM layer

4. Concrete shows no degradation due to microcracking

5. Steel fibers are considered to have a uniform cross-section along fiber length

6. Representative Volume Element (RVE) periodicity assumption is considered for SFRC

Fatigue life modelling

The fatigue life of the Cement Asphalt Mortar (CAM) layer is evaluated using a stress-based S–N relationship derived from experimental studies on cementitious composite materials subjected to cyclic loading. This approach is widely adopted for materials that exhibit quasi-brittle behavior under repeated loading. The fatigue life is expressed as:

$$\log(N) = -10.319\,S + 11.567$$

where Nrepresents the number of load cycles to failure, and $S$is the normalized stress amplitude defined as $S = \sigma_a / f_u$. Here, $\sigma_a$is the applied compressive stress obtained from the finite element (FE) analysis, and $f_u$denotes the compressive strength of the CAM material.

The maximum compressive stress in the CAM layer, obtained from the coupled thermo-mechanical dynamic analysis, is used as the governing stress parameter for fatigue life estimation. This method represents a conservative approach, assuming that the CAM layer is repeatedly loaded to the peak stress level throughout its service life.

Both stress amplitude and loading frequency strongly influence the fatigue performance of CAM. An increase in stress amplitude accelerates the initiation and propagation of microcracks within the material, thereby significantly reducing fatigue life. Additionally, due to CAM's viscoelastic nature, loading frequency plays a critical role in its mechanical response. At higher loading frequencies, such as those associated with high-speed rail operations (~30 Hz), the material exhibits relatively stiffer behavior due to limited time for viscous deformation, which affects stress distribution and fatigue characteristics. Conversely, lower loading frequencies allow greater viscoelastic relaxation, potentially resulting in increased deformation accumulation.

RESULTS AND DISCUSSIONS:

Dynamic and heat transfer analysis

The passage of a high-speed train results in forces that cause stresses, deformations, and possible damage to the pre-cast slab track. Track parameters, e.g., rail irregularities, can amplify these forces. Temperature gradients

due to atmospheric radiation can cause additional stresses. Therefore, the adopted modeling approach was sequential coupling. It accounted for dynamic forces on the track due to vehicle-track interaction, which are amplified by imperfections such as track irregularities. It also accounted for the effect of temperature gradients on the slab stresses. Figs. 2(a) and (b) represent the dynamic forces on the track due to vehicle-track interaction for vertical and lateral rail-wheel force, respectively.

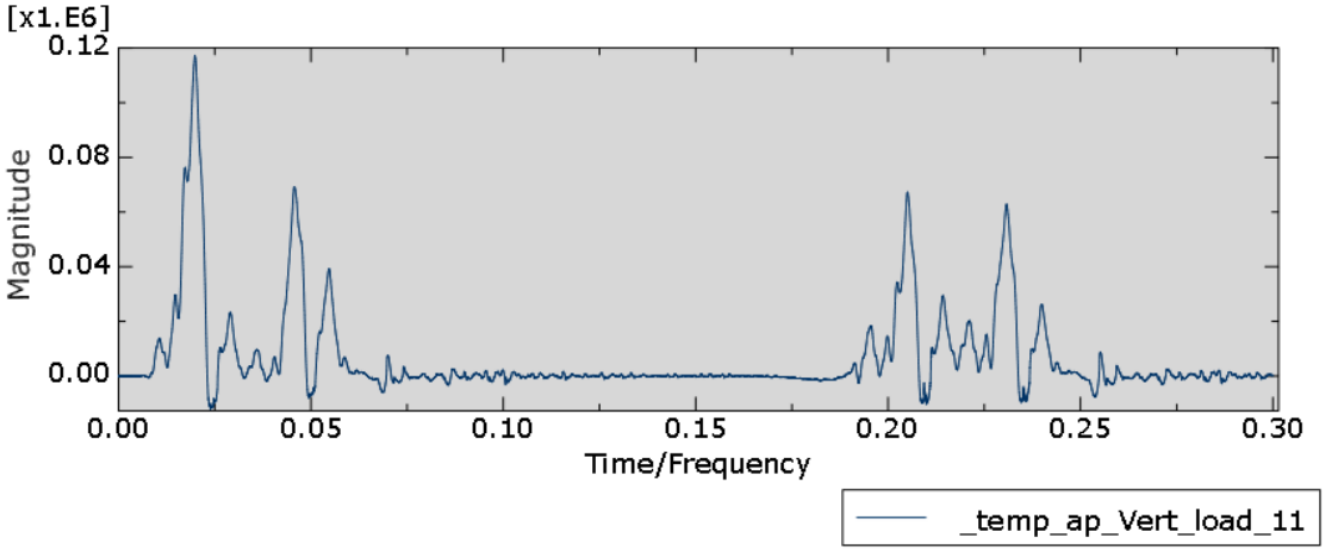

(a)

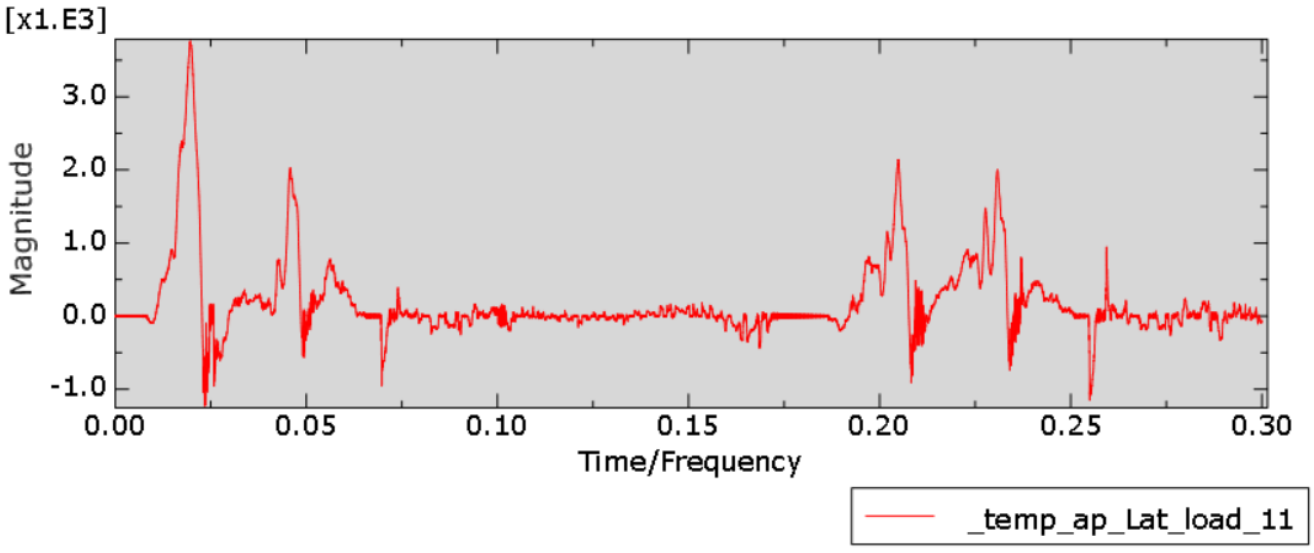

(b)

Figure 2: Dynamic forces in Rail-wheel tracks. (a) Vertical and (b) Lateral

A heat transfer analysis is performed using ABAQUS at the peak of summer in Ahmedabad. Meteorological data was taken on 25th May, 2020. Peak temperature was 45 $^{\circ}$C. Average wind speed for the day is 3.7 m/s. The heat transfer analysis accounted for the effect of incident solar radiation and convective heat transfer. Atmospheric temperature and wind speed were modelled using appropriate thermal boundary conditions. Fig. 3 represents the temperature gradients in the slab due to atmospheric temperature variations. Fig. 3 shows that there is a critical time at which the temperature difference between the top and bottom surfaces of the concrete slab is at its maximum.

The goal of the dynamic analysis is to determine the maximum stress in the track slab induced by rail-wheel forces. The maximum stress value is used to determine the fatigue life of the CAM when subjected to stresses of the same magnitude over repeated cycles. The maximum compressive stress obtained from the dynamic

analysis in the CAM was 0.3108 MPa (Fig. 3). This stress value was subsequently used to determine the fatigue life of the CAM layer.

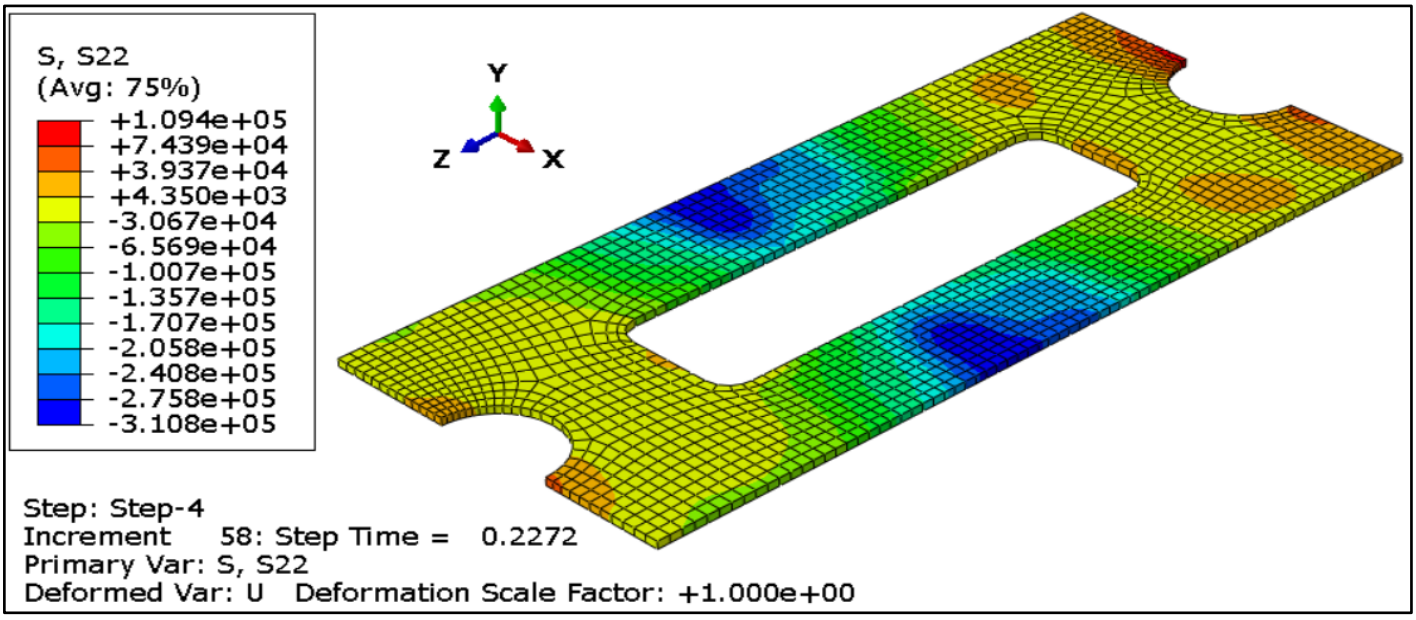

Figure 3: Normal Stress (MPa) Contour in CAM layer along its depth

Interface damage between the concrete slab and CAM layer

The SDEG (scalar stiffness degradation) is specified as the damage status of the interface elements used in the cohesive element in the Abaqus field output. When the interface stress reaches its maximum strength, the SDEG value exceeds 0. When the interface is completely damaged, the SDEG value equals 1. The distribution of SDEG contours is shown in Fig. 4. The red part indicates a completely cracked slab-CAM interface. It shows that interface failures occur mainly at the corners and near the boundary.

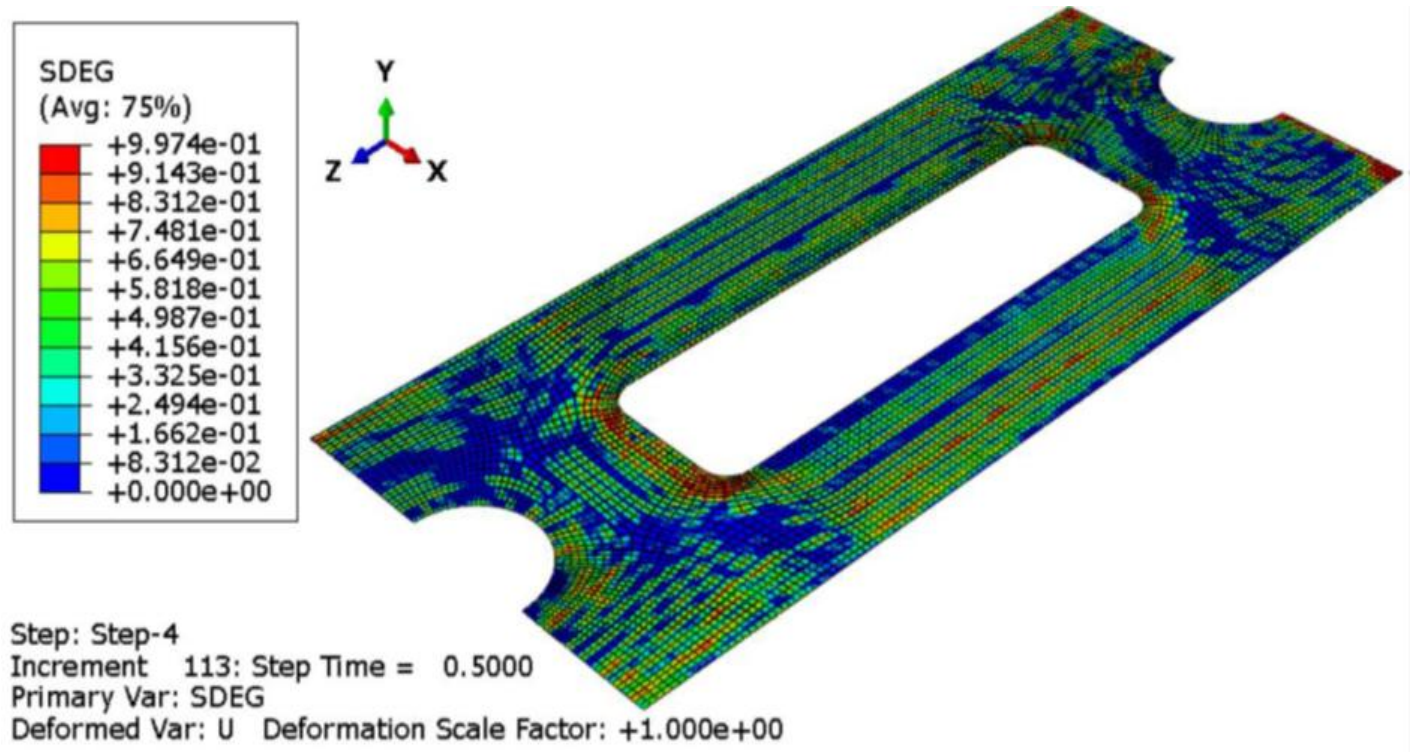

Figure 4: SDEG Contour for a cohesive layer at the end of analysis

3.3 Damage in Concrete Slab

The tensile damage parameter, DAMAGET, is defined as the ratio of cracking strain to total strain. The compressive damage parameter, DAMAGEC, is defined similarly as the ratio of inelastic strain to total strain. Fig. 5 (a)-(c) shows the contours of compression damage, tension damage, and SDEG for a concrete slab, respectively. It can be seen that the damage to the concrete slab itself is negligible compared to the damage at the interface between the slab and the CAM layer.

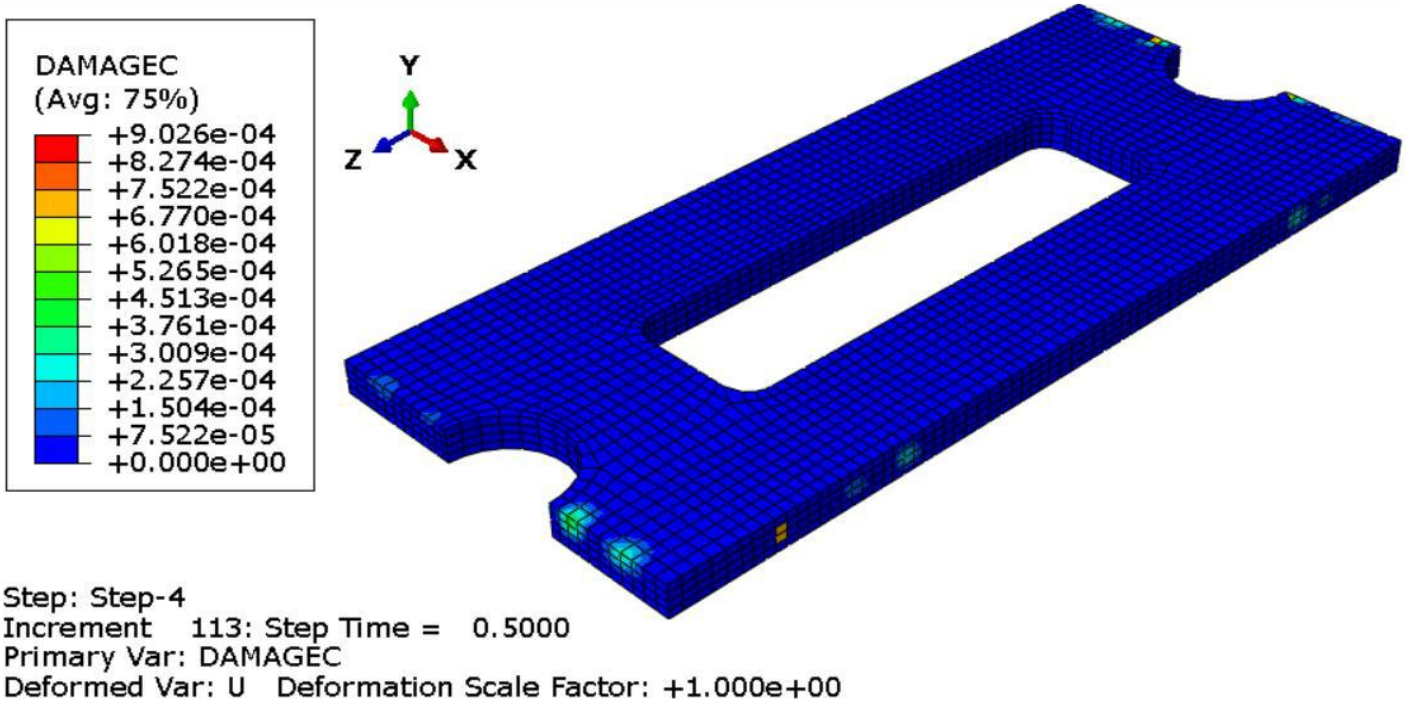

(a)

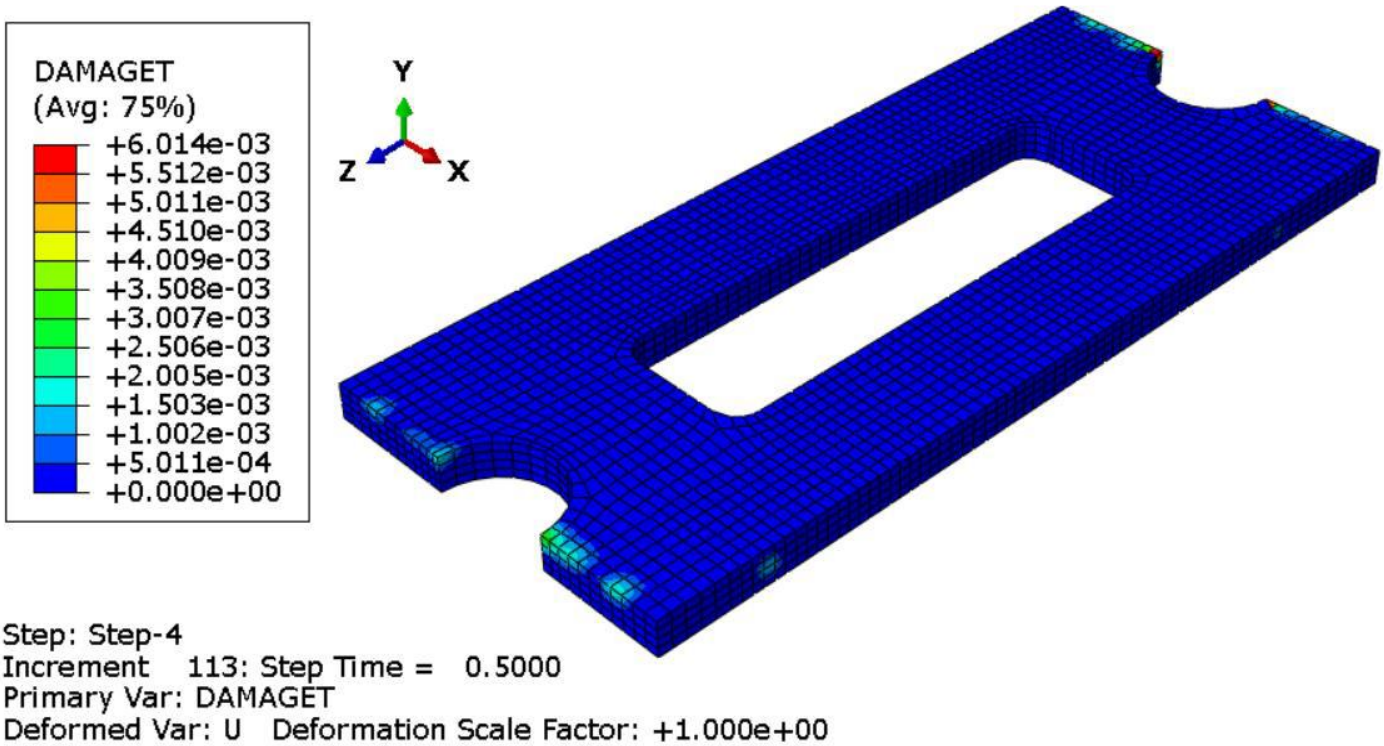

(b)

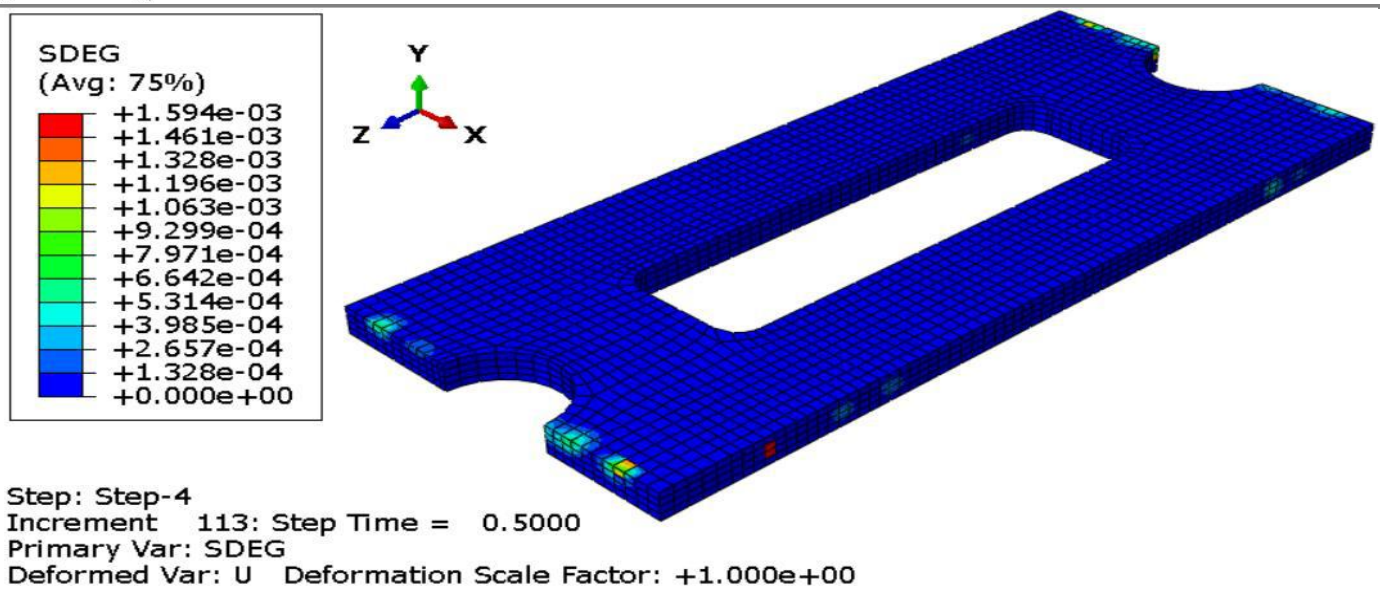

(c)

Figure 5: (a) Compression damage contour in a concrete slab at the end of analysis, (b)Tension damage contour in a concrete slab at the end of analysis, and (c) SDEG contour of concrete slab at the end of analysis

Displacement of track slab

Fig. 6 (a) and (b) plot contours of the vertical and lateral displacement throughout the track slab at the time instants when the vertical and lateral displacements achieve their peak values. It can be observed that the peak values are well within the allowable limits specified by NHSRAI. According to NHSRAI the track slab must satisfy the following criteria:

1. Limit on vertical deformation of track slab: The absolute limit or relative limit on the vertical deformation will be 10 mm for a 10 m length of the slab track.

2. The maximum horizontal track slab displacements shall not exceed 6mm for a 10 m length of the slab track.

Moreover, the contour of the vertical displacement reveals a higher magnitude near the center of the concrete slab.

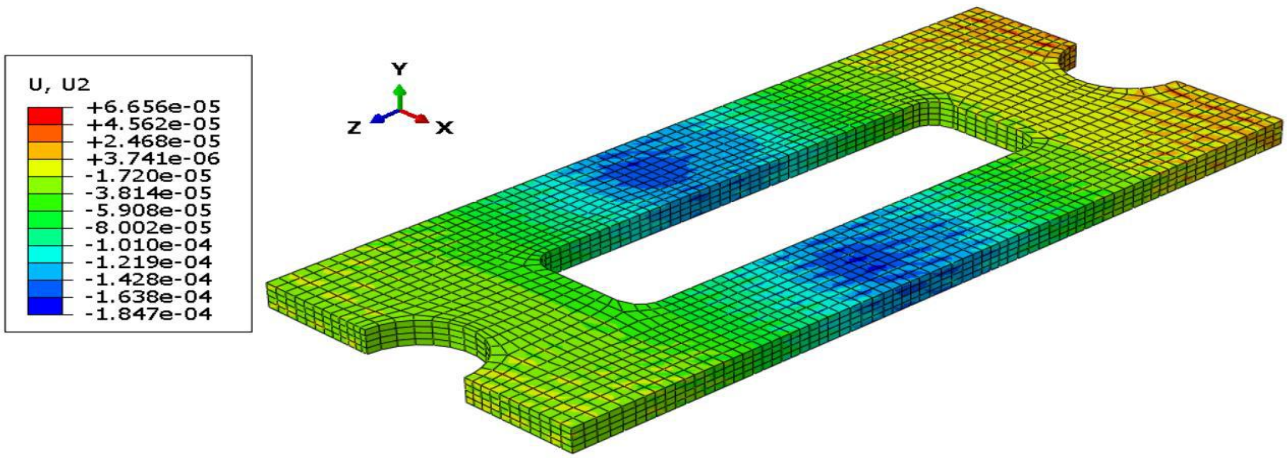

(a)

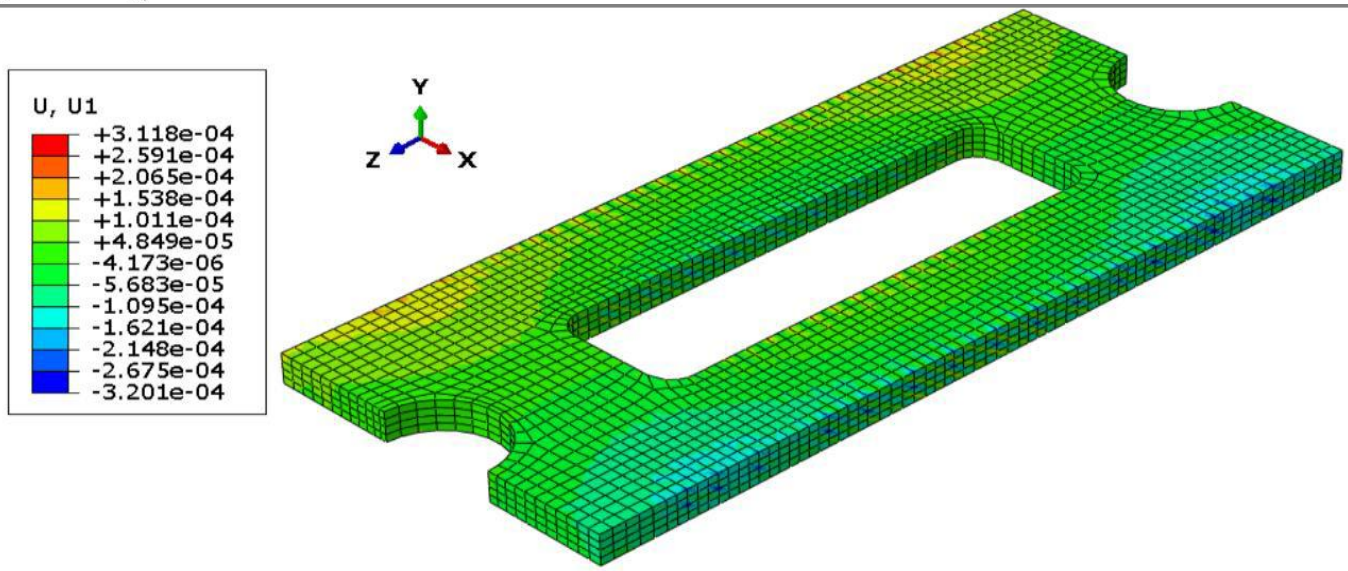

(b)

Figure 6: Displacement in concrete slab. (a) Vertical and (b) Lateral

The critical nodes, i.e., the nodes with the largest vertical displacement and largest lateral displacement, are determined from Fig. 6 (a) and (b).

Dynamic response of SFRC slab track

A hollow-shell model of a concrete slab is created, steel fibers with shifted coordinates are placed within it, and penetrations are resolved using the Abaqus contact algorithm. The final fiber configuration is shown in Fig. 7. The entire simulation for the track slab was re-performed with the rebars replaced by random steel fibers.

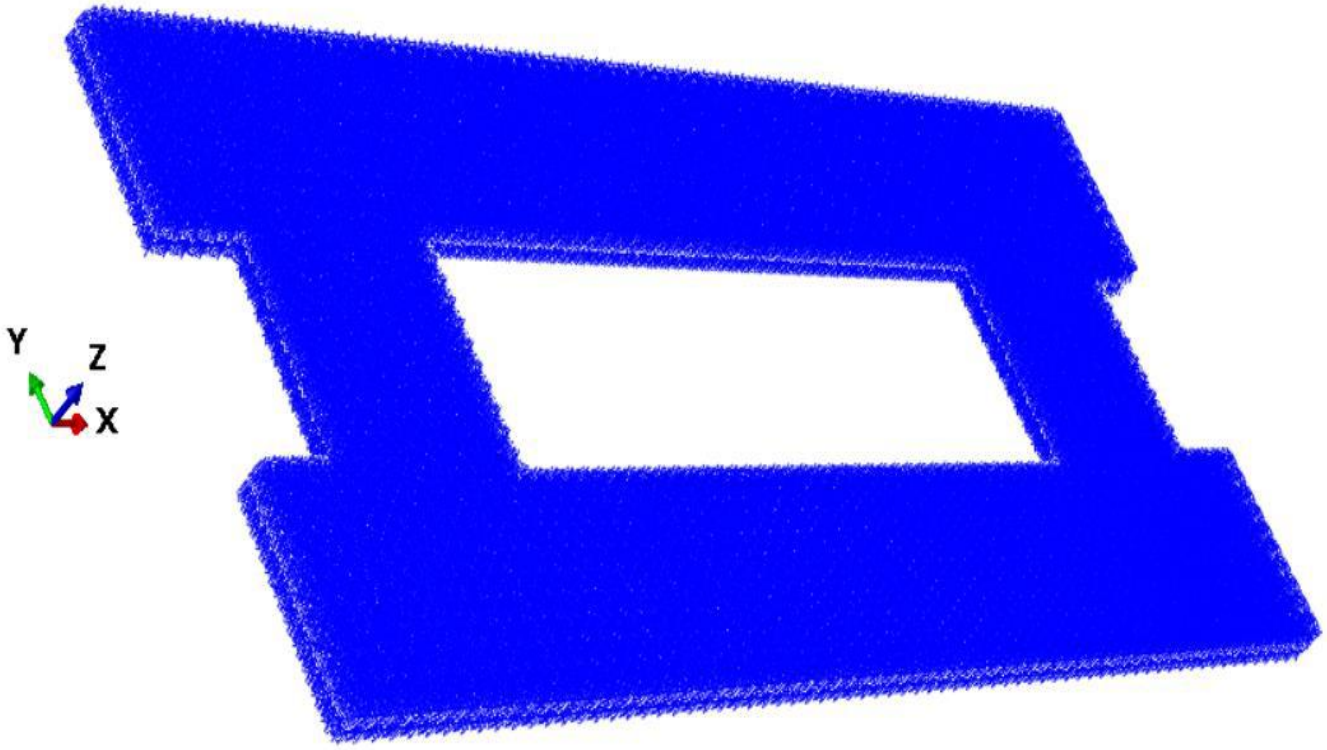

Figure 7: Steel fibers duplication after adjustments in the concrete slab

Compressive Fatigue Life Calculation of CAM Layer

The maximum compressive stress in CAM, as determined by the above analysis, was 0.2196 MPa. The fatigue life of CAM is calculated for σ_a = 0.22 MPa and 30 Hz loading frequency. Fig. 8 shows the normal stress contour in the CAM layer along its depth.

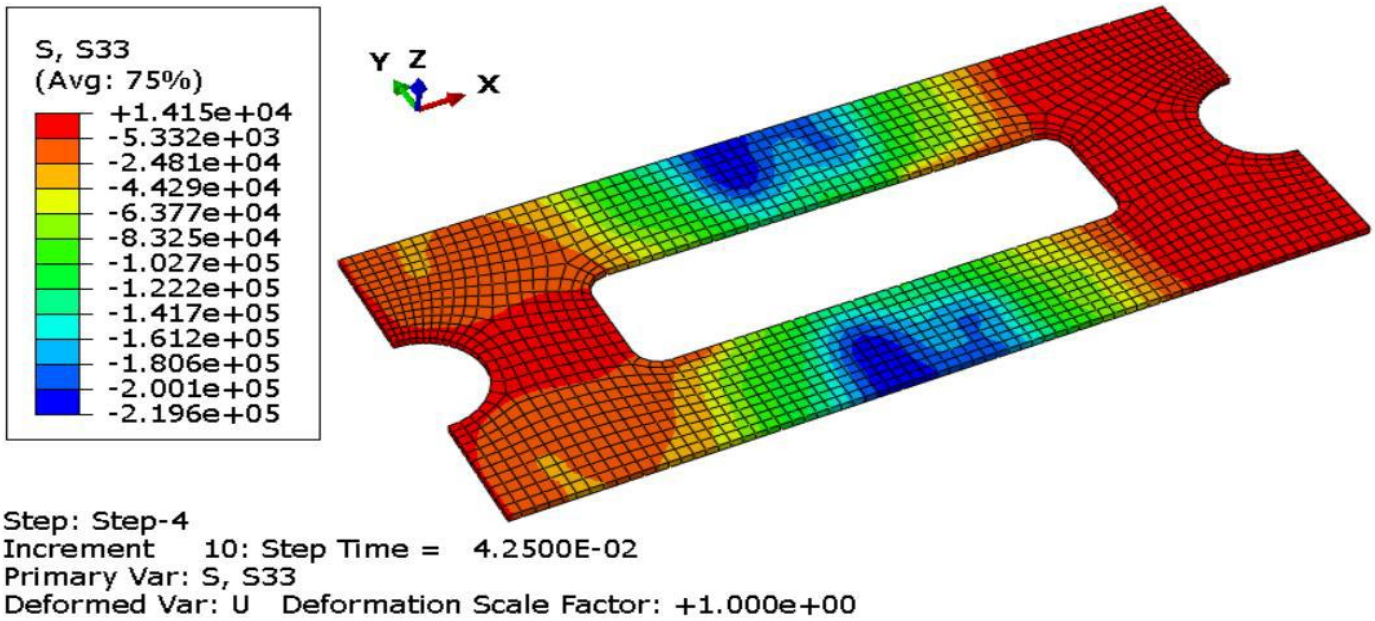

Figure 8: Normal Stress (MPa) Contour in CAM layer along its depth

Interface Damage between SFRC and CAM Layer

The SDEG contour for the interface between the SFRC and the CAM layer is shown in Fig. 9. Replacing regular bars with steel fibers results in slightly higher interface damage, though the difference is not significant.

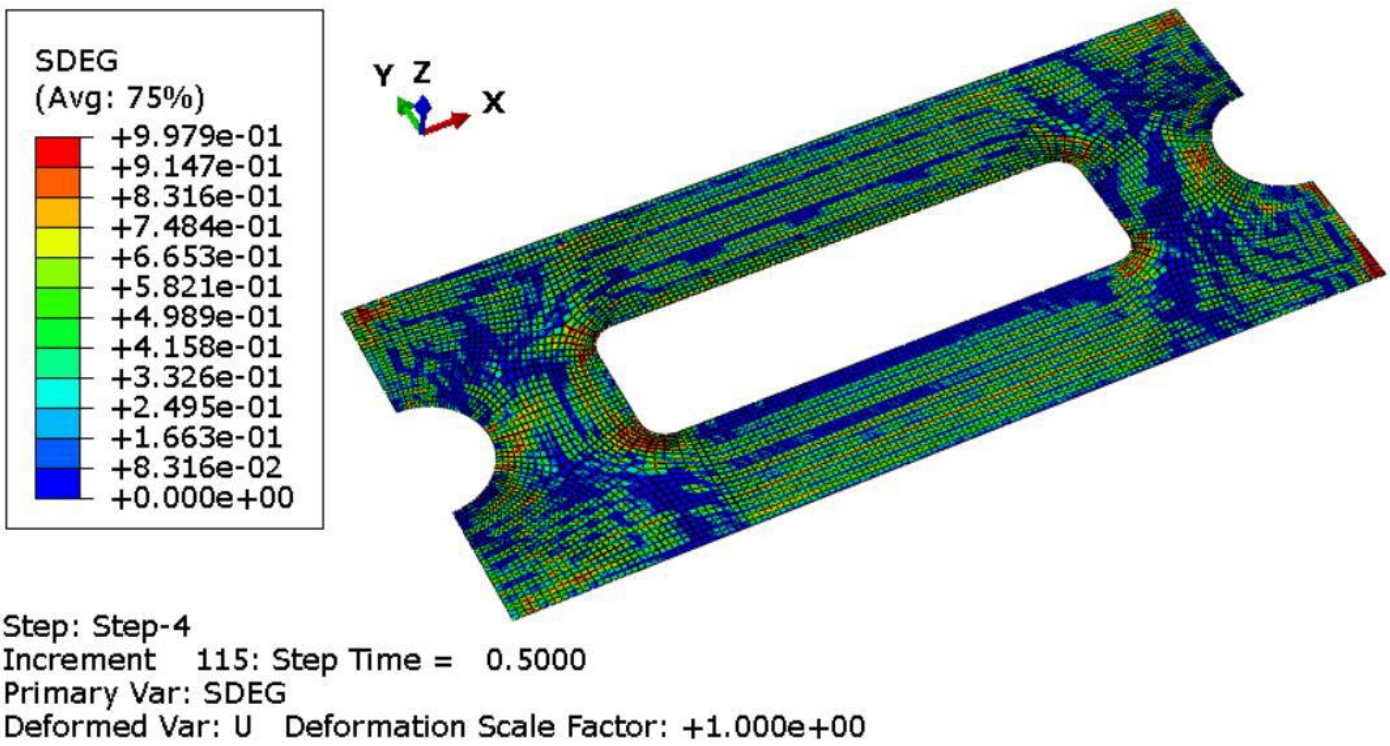

Figure 9: SDEG Contour of cohesive layer at the end of analysis

Displacement Contour of SFRC slab

The maximum vertical and lateral displacement of the prestressed concrete slab are 0.1144 mm (Fig. 10 (a)) and 0.2833 mm (Fig. 10 (b)), respectively, which are well within the acceptable limit given by the National High-speed Rail Authority of India.

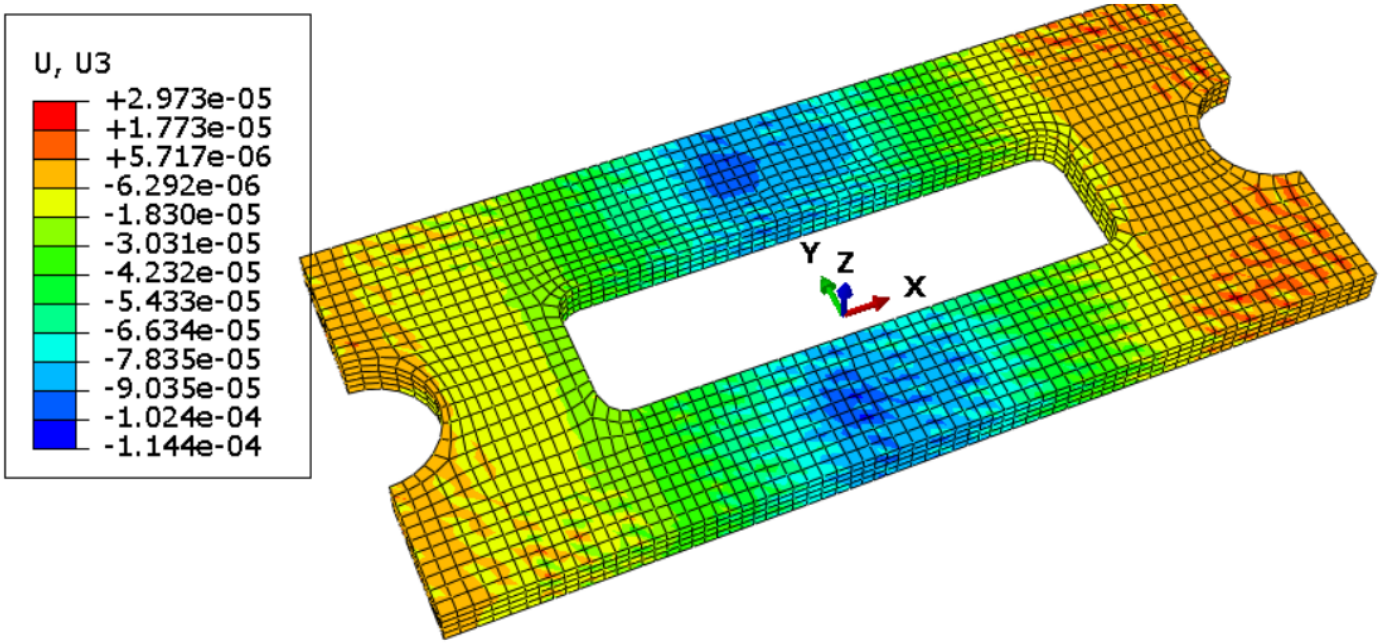

(a)

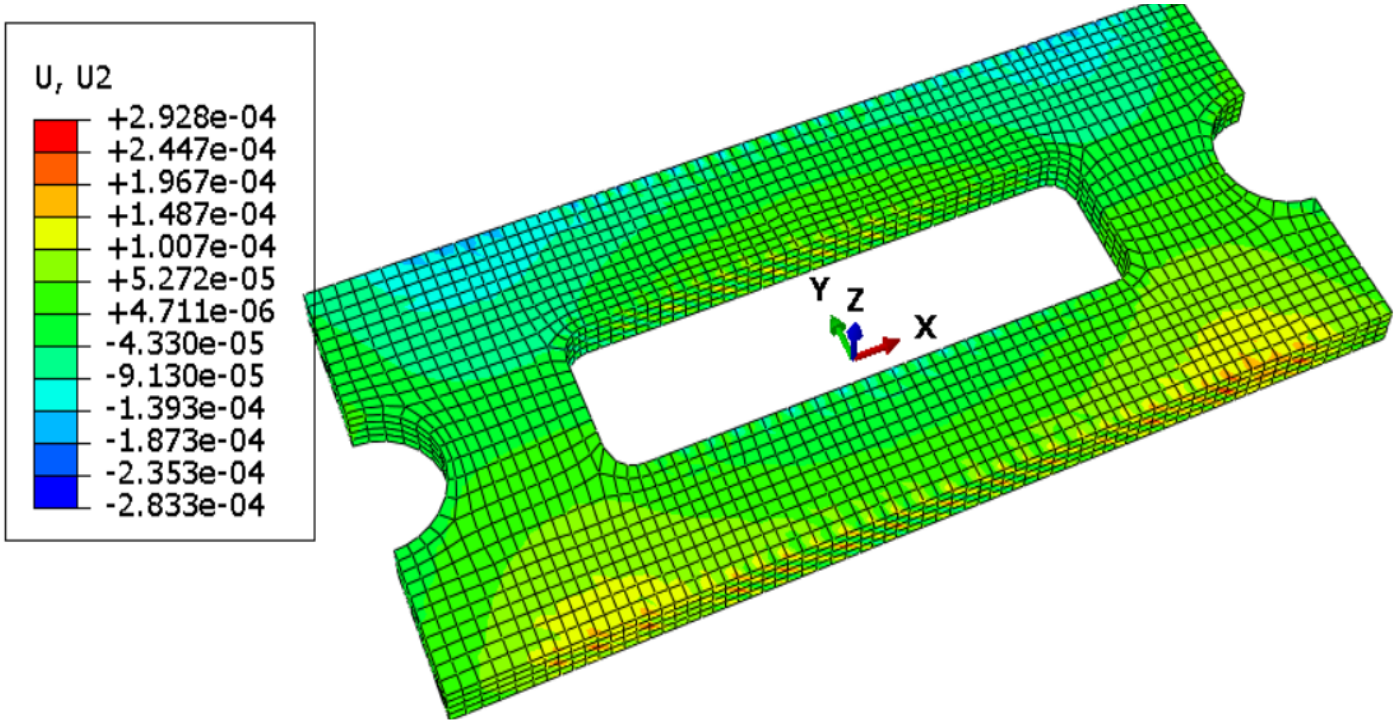

Figure 10: Displacement contour in SFRC slab (m). (a) Vertical, and (b) Lateral

Performance Comparison

A final comparison of the performance of the SFRC slab and the slab with ordinary rebars is included in Table 1. As is apparent, for almost all diagnostics, the SFRC slab performs better than the slab with ordinary rebars.

Table 1: Assessment of the SFRC slab's performance versus that of a slab made with conventional rebars

Diagnostic	Steel fibers in prestressed concrete slab	Ordinary reinforced prestressed concrete slab	Design/Allowable limits
Maximum compressive stress in CAM layer	0.22 MPa	0.31 MPa	Nil
Total plastic deformation in CAM Layer caused by loading after 50 years	0.138 mm	0.187 mm	0.4 mm
Maximum vertical displacement of the slab	0.1144 mm	0.1847 mm	10mm/10m slab length
Maximum lateral displacement of the slab	0.2928 mm	0.3201 mm	6mm/10m slab length
Maximum Interface SDEG	0.9979	0.9974	
Maximum SDEG in Slab	1.044 E-03	1.594 E-03	
Maximum Compressive damage in the slab	5.351 E-04	9.026 E-04	
Maximum Tensile damage in the slab	1.558 E-03	6.014 E-03	

CONCLUSIONS

This study presents a detailed numerical analysis of the dynamic and thermo-mechanical response of non-ballasted slab track systems incorporating CAM and SFRC under realistic high-speed rail operating conditions. The developed finite element framework successfully captures the coupled effects of moving loads, thermal gradients, and material nonlinearity, providing valuable insights into track performance and durability.

The results confirm that the CAM layer exhibits excellent fatigue resistance, with a predicted life exceeding 167 million axle repetitions under a maximum compressive stress of 0.31 MPa, far surpassing typical design requirements. Replacement of conventional reinforcement with SFRC significantly improves system performance by reducing CAM compressive stress by approximately 29% and lowering long-term plastic deformation by nearly 26%. Additionally, SFRC slabs exhibit greater structural integrity, with substantial reductions in tensile and compressive damage compared to traditional reinforced concrete slabs.

ACKNOWLEDGEMENT

The authors would like to acknowledge the funding support received from Anusandhan National Research Foundation (ANRF) under Partnerships for Accelerated Innovation and Research (PAIR) with IIT(ISM) Dhanbad for the project "Development of Innovative and Cutting-Edge Indigenous Technologies for Critical Minerals Exploration and Smart/Sustainable Mining", Sanction order no. ANRF/PAIR/2025/000027/PAIR-B.

Data availability statement:

The authors declare that the data supporting the findings of this study are available within the paper. There is no additional data to support the study's findings.

Nomenclature:

CAM	Cement Asphalt Mortar	PSD	Power spectral density
FEM	Finite element method	RVE	Representative volume element
HSR	High-speed rail	SFRC	Steel fiber reinforced concrete
ITZ	Interfacial transition zones	UHPC	Ultra-high performance concrete

REFERENCES

1. R. Mu, S. Mei, J. Chen, X. Wang, N. Liu, X. Chen, L. Qing, and Y. Shi, "Effect of steel fiber orientation on punching shear resistance of steel fiber reinforced cementitious composites round slabs," J. Build. Eng., vol. 89, no. December 2023, 2024, doi: 10.1016/j.jobe.2024.109289.
2. Y. Wang, P. Qiao, J. Sun, and A. Chen, "Influence of fibers on tensile behavior of ultra-high performance concrete: a review," Constr. Build. Mater., vol. 430, no. November 2023, p. 136432, 2024, doi: 10.1016/j.conbuildmat.2024.136432.
3. S. Hou, K. Li, X. Hu, and C. Shi, "Assessment on the heterogeneity and roughness of fracture surface of steel fiber reinforced concrete," Constr. Build. Mater., vol. 438, no. February, p. 137025, 2024, doi: 10.1016/j.conbuildmat.2024.137025.
4. J. Xue, S. Mao, P. Cacciola, A. Contento, A. Lampropoulos, D. Nicolaides, M. F. Petrou, Z. Yang, and B. Briseghella, "Experimental evaluation of the effectiveness of fiber orientation methods on the mechanical performance of UHPFRC," Constr. Build. Mater., vol. 448, no. 2, p. 138184, 2024, doi: 10.1016/j.conbuildmat.2024.138184.
5. Y. Yang, P. Lu, Z. Liu, L. Dong, J. Lin, T. Yang, Q. Ren, and C. Wu, "Effect of steel fibre with different orientations on mechanical properties of 3D-printed steel-fibre reinforced concrete: Mesoscale finite element analysis," Cem. Concr. Compos., vol. 150, no. April, p. 105545, 2024, doi: 10.1016/j.cemconcomp.2024.105545.
6. H. Zhang, L. Cao, Y. Duan, Z. Tang, F. Hu, and Z. Chen, "High-flowable and high-performance steel fiber reinforced concrete adapted by fly ash and silica fume," Case Stud. Constr. Mater., vol. 20, no. November 2023, p. e02796, 2024, doi: 10.1016/j.cscm.2023.e02796.
7. W. Zhang, J. Tian, X. Wu, Y. Zheng, Y. Zuo, K. Gao, W. Wang, and W. Huang, "Investigation of basic properties, microscopic characteristics, and optimized ratio prediction model of ultra-high steel fiber reinforced concrete," Case Stud. Constr. Mater., vol. 20, no. April, p. e03297, 2024, doi: 10.1016/j.cscm.2024.e03297.
8. M. Zhou, X. He, H. Wang, W. Wu, J. He, and C. Wu, "Experimental study of mechanism properties of interfacial transition zones in steel fiber reinforced concrete," Case Stud. Constr. Mater., vol. 20, no. November 2023, p. e02954, 2024, doi: 10.1016/j.cscm.2024.e02954.
9. Z. Jia, M. Zhou, Y. Chen, W. Wang, L. Ma, Y. Chen, C. Liu, and Y. Zhang, "Effect of steel fiber shape and content on printability, microstructure and mechanical properties of 3D printable high strength cementitious materials," Case Stud. Constr. Mater., vol. 20, no. December 2023, p. e03080, 2024, doi: 10.1016/j.cscm.2024.e03080.
10. S. Liu, X. Wang, Y. Li, and Y. Liu, "Stress-strain relationship of airfoiled-shaped milled-cut steel fiber-reinforced concrete under uniaxial compression: Experiments and analytical model," Case Stud. Constr. Mater., vol. 21, no. September, 2024, doi: 10.1016/j.cscm.2024.e03925.
11. K. Yang, Z. Wu, K. Zheng, and J. Shi, "Shear behavior of regular oriented steel fiber-reinforced concrete beams reinforced with glass fiber polymer (GFRP) bars," Structures, vol. 63, no. April, p. 106339, 2024, doi: 10.1016/j.istruc.2024.106339.
12. Y. Zheng, X. Lv, S. Hu, J. Zhuo, C. Wan, and J. Liu, "Mechanical properties and durability of steel fiber reinforced concrete: A review," J. Build. Eng., vol. 82, no. November 2023, p. 108025, 2024, doi: 10.1016/j.jobe.2023.108025.
13. M. Rashidi, S. Kargar, and S. Roshani, "Experimental and numerical investigation of steel fiber concrete fracture energy," Structures, vol. 59, no. August 2023, p. 105792, 2024, doi: 10.1016/j.istruc.2023.105792.
14. D. Jayasooriya, P. Rajeev, and J. Sanjayan, "Tensile stress-strain models for steel fiber reinforced concrete," J. Build. Eng., vol. 96, no. August, p. 110533, 2024, doi: 10.1016/j.jobe.2024.110533.
15. F. Altheoy, O. Zaid, B. Ahmed, and K. M. Elhadi, "Impact of double hooked steel fibers and nano-kaolin clay on fresh properties of 3D-Printable ultra-high-performance fiber-reinforced concrete," J. Build. Eng., vol. 97, no. September, p. 110917, 2024, doi: 10.1016/j.jobe.2024.110917.
16. L. Yu, Y. Liu, and Y. Liu, "Advanced monitoring of damage behavior and 3D visualization of fiber distribution in assessing crack resistance mechanisms in steel fiber-reinforced concrete," J. Build. Eng., vol. 97, no. October, 2024, doi: 10.1016/j.jobe.2024.110980.
17. M. Yang, Y. Xiong, X. Shang, Z. Wang, J. Zhao, Y. Liu, and Y. Yuan, "Effect of steel fibers on the

stress–strain behavior of aligned steel fiber ultra-high performance concrete under uniaxial compression," J. Build. Eng., vol. 98, no. July, p. 111092, 2024, doi: 10.1016/j.jobe.2024.111092.

18. F. Liu, Y. Li, J. Lv, Y. Liu, H. Li, and F. Mu, "Uniaxial compression performance of SIFCON with the arc-shaped steel fibers," J. Build. Eng., vol. 100, no. September 2024, p. 111678, 2025, doi: 10.1016/j.jobe.2024.111678.
19. E. A. H. Alwesabi, B. H. A. Bakar, I. M. H. Alshaikh, A. M. Zeyad, A. Altheeb, and H. Alghamdi, "Experimental investigation on fracture characteristics of plain and rubberized concrete containing hybrid steel-polypropylene fiber," Structures, vol. 33, no. January, pp. 4421–4432, 2021, doi: 10.1016/j.istruc.2021.07.011.
20. J. Ren, J. Wang, X. Li, K. Wei, H. Li, and S. Deng, "Influence of cement asphalt mortar debonding on the damage distribution and mechanical responses of CRTS I prefabricated slab," Constr. Build. Mater., vol. 230, p. 116995, 2020, doi: 10.1016/j.conbuildmat.2019.116995.